TECHNICAL UNIVERSITY OF LIBEREC
Faculty of Mechatronics, Informatics
and Interdisciplinary Studies

Extended Finite Element Methods for Approximation of Singularities

Extended Abstract of the Doctoral Thesis

Study programme:	P3901 – Applied Sciences in Engineering
Study branch:	3901V055 – Applied Sciences in Engineering
Author:	**Ing. Pavel Exner**
Supervisor:	doc. Mgr. Jan Březina, Ph.D.

Liberec

Abstrakt

Tato doktorská práce je zaměřena na řešení problému proudění podzemní vody v porézním prostředí, které je ovlivněno přítomností vrtů či studní. Model proudění je sestaven na základě konceptu redukce dimenzí, který je hojně využíván při modelování rozpukaného porézního přostředí, především granitů. Vrty jsou modelovány jako 1d objekty, které protínají blok horniny. Propojení těchto domén v redukovaném modelu způsobuje singularity v řešení v okolí vrtů. Vrty i porézní médium jsou síťovány nezávisle na sobě, což vede k výpočetním sítím kombinujícím elementy různých dimenzí.

Jádrem doktorské práce je pak vývoj specializované metody konečných prvků pro výše popsaný model. Pro umožnění propojení sítí různých dimenzí a pro zpřesnění aproximace singularit v okolí vrtů je použita rozšířená metoda konečných prvků (XFEM), v rámci níž jsou navrženy nové typy obohacení konečně-prvkové aproximace. Metoda XFEM je nejprve aplikována v modelu pro tlak, dále je navrženo obohacení pro rychlost a metoda je použita ve smíšeném modelu, jehož řešením jsou rychlost i tlak.

Doktorská práce se dále detailně věnuje numerickým aspektům v metodě XFEM, a to především adaptivním kvadraturám, volbě velikosti obohacené oblasti nebo podmíněnosti výsledného lineárního systému. Vlastnosti navržené XFEM metody a optimální konvergence jsou ověřeny na sérii numerických experimentů. Praktickým výstupem doktorské práce je implementace metody XFEM jako součásti open-source softwaru Flow123d.

Klíčová slova: Rozšířená metoda konečných prvků (XFEM), singularita, sítě kombinovaných dimenzí, Darcyho proudění, rozpukané porézní prostředí

Abstract

In this doctoral thesis, a model of groundwater flow in porous media influenced by wells (boreholes, channels) is developed. The model is motivated by the reduced dimension approach which is being often used in fractured porous media problems, especially in granite rocks. The wells are modeled as lower dimensional 1d objects and they intersect the surrounding bulk rock domains. The coupling between the wells and the rock then causes a singular behavior of the solution in the higher dimensional domains in the vicinity of the cross-sections. The domains are discretized separately resulting in an incompatible mesh of combined dimensions.

The core contribution of this work is in the development of a specialized finite element method for such model. Different Extended finite element methods (XFEM) are studied and new enrichments are suggested to better approximate the singularities and to enable the coupling of the wells with the higher dimensional domains. At first the XFEM is applied in a pressure model, later an enrichment for velocity is suggested and the XFEM is used in a mixed model, solving both velocity and pressure.

Different numerical aspects of the XFEM is studied in details, including an adaptive quadrature strategy, a proper choice of the enrichment zone or a conditioning of the resulting linear system. The properties of the suggested XFEM are validated on a set of numerical tests and the optimal convergence rate is demonstrated. The XFEM is implemented as a part of the open-source software Flow123d.

Keywords: Extended Finite Element Method (XFEM), Singularity, Meshes of combined dimensions, Darcy flow, Fractured porous media

Contents

List of Figures

List of Tables

List of Graphs

List of Abbreviations and Symbols

Acronyms

DFN	Discrete Fracture Network
FEM	Finite Element Method
XFEM	Extended Finite Element Method
GFEM	Generalized Finite Element Method
SGFEM	Stable Generalized Finite Element Method
FLOP	Floating Point Operation
AABB	Axes Aligned Bounding Boxes
BIH	Boundary Interval Hierarchy
IC,IP	Intersection Corner, Intersection Polygon

V_h	discrete space of the primary variable
Q_h	discrete space of the secondary variable
Λ_h	discrete space of Lagrange multipliers
d	dimension: 1d, 2d, 3d
Ω_d	domain of dimension d
Γ_{dN}	part of boundary of Ω_d with Neumann b.c.
Γ_{dD}	part of boundary of Ω_d with Dirichlet b.c.
$\mathcal{T}_d$	mesh consisting of elements of dimension d
$\mathcal{F}_d$	faces of elements in $\mathcal{T}_d$
h	mesh parameter
T_d^i, F_d^i	element and face of $\mathcal{T}_d$
$\mathcal{I}_{dE}, \mathcal{I}_{dF}, \mathcal{I}_{dN}$	indices of elements, faces and nodes in $\mathcal{T}_d$
$\mathcal{J}_{dE}, \mathcal{J}_{dN}$	indices of enriched elements and nodes in $\mathcal{T}_d$
Ω_C^w	domain (cylinder) of a well w
Ω_1^w	reduced domain (line) of a well w
Γ_w^m	interface boundary between well w and aquifer m
$\mathcal{W}$	index set of wells
$\mathcal{M}$	index set of aquifers
p_d	pressure in d-dimensional domain
$\boldsymbol{u}_d$	velocity in d-dimensional domain
λ_d	Lagrange multipliers in d-dimensional domain
$\boldsymbol{n}$	(outward) normal unit vector
δ_d	cross-section of d-dimensional domain
f_d	source term in d-dimensional domain
g_{dD}	Dirichlet b.c. in d-dimensional domain
g_{dN}	Neumann b.c. in d-dimensional domain
σ_w, σ_w^m	permeability coefficient between well and aquifer
r_w, ρ_w, R_w	distance function, radius and enrichment radius
Z_w	enrichment zone of a well w
$s_w, \boldsymbol{s}_w$	scalar and vector global enrichment function
$a(\cdot,\cdot)$	bilinear form
$l(\cdot)$	linear form
$\left\|\cdot\right\|_V$	norm associated to a space V
$\langle\cdot\rangle$	average operator
$\{\cdot\}$	fluctuation operator
π_T, π_T^{RT}, π_h	interpolation operators

1 Introduction

A large set of problems with finite element models, that people nowadays deal with, is connected with insufficient accuracy in cases where the model includes large and very small scale phenomena at once. One can imagine a simulation of groundwater flow in a large domain (hundreds of meters or even kilometers) which can be significantly influenced by thin fractures in the porous media or artificial wells and boreholes (several centimeters in diameter). These disturbances bring discontinuities and singularities into the model which are hard to capture at the geometric level and even harder to approximate with the standard polynomial finite elements (FE) at the discretization level. There are several ways one can follow to increase the accuracy of the standard finite element method FEM in such models.

Adaptive meshes can be used in such cases, but it can cost a lot of computational power to build a very fine mesh, and then solve the problem with increasing number of degrees of freedom. It requires very robust meshing algorithms when complex geometries are in question. There can be other constraints on the mesh generation in specific applications: mesh elements quality, presence of hanging nodes, compatible meshes. Considering time dependent problems, such as an opening of fractures in mechanics, remeshing at each time step is required which further amplifies the demands on the meshing tools. All these aspects make the generation of computational meshes hard or even close to impossible.

Alternatively, a reduced dimension concept is often used and models combining different dimensions are developed. The geometry is decomposed in objects of different dimensions (2d fractures, 1d wells, 0d point sources) and the meshes of these domains are created independently. Later the modeled processes must be coupled between the domains of different dimensions. The coupling concepts are mostly available at the continuous level but their implementation at the discrete level is non-trivial and problems often appear there. Two types of meshes are used in these models: compatible and incompatible. An incompatible mesh is the one, where the intersections of the computational domains are not aligned to nodes and sides of elements. Such meshes with arbitrary intersections are easier to construct, but bring a whole new set of problems in the coupling.

Finally, there are the Extended finite element methods (XFEM). The XFEM enables us to take advantage of an a priori knowledge of the model solution character such as discontinuity or singularity of searched quantities. The key aspect of the XFEM is that it allows to locally incorporate non-polynomial functions, like a jump or a singular function, into the finite element solution in places, where these features are expected to appear. This way the standard finite element approximation space is extended (enriched) and it is able to approximate the small scale phenomena more accurately. See an example of XFEM usage in 1d-2d coupling with point intersections in Figure 1.1.

This thesis is aimed at further development of the XFEM and its usage in reduced dimensional models in groundwater flow problems, especially in non-planar 1d-2d and 1d-3d coupling. The incompatible meshes are considered and the XFEM is used to glue the modeled processes in different dimensions back together. A model is searched that fits in the concept of the software Flow123d, which is being developed at the Technical University of Liberec.

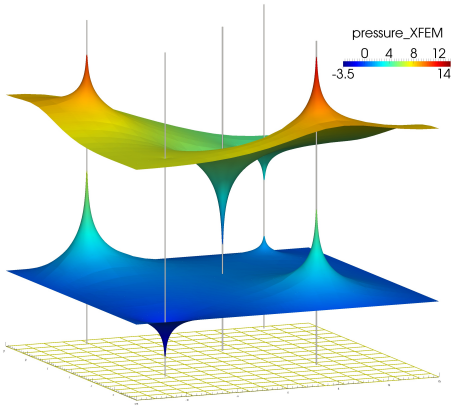

Figure 1.1: An XFEM example in 1d-2d coupling with singularities at intersection points. Distribution of pressure in 2 aquifers (horizontal planes) intersected by 5 wells (vertical lines) is displayed. The model is computed on a coarse mesh without refinement (visible at the bottom).

1.1 Flow123d

The practical outcome of this thesis is a new model and its solver implemented as a part of the software Flow123d. Flow123d, last version 2.2.1 released in 2018 [1], is a simulator of underground water flow, solute and heat transport in fractured porous media. The software is developed as an open source code under the versioning system Git where the eponymous project can be found, or one can reach it via the web page `http://flow123d.github.io`.

The main feature of the software is the ability to compute on complex compatible meshes of combined dimensions, where the continuum models and discrete fracture network models can be coupled. Only the coupling of co-dimension 1 is considered, i.e. coplanar 1d-2d and 2d-3d cases. This thesis extends the groundwater flow model to non-planar 1d-2d and 1d-3d coupling.

1.2 Aims of Thesis

The aims of the thesis are in further development of reduced dimensional FEM models, especially of co-dimension 2, in combination with the XFEM and incompatible meshes, where the XFEM provides a way for coupling the domains of different dimensions together and to significantly improve the finite element approximation accuracy.

The research aims can be summarized in two major points

- Propose suitable XFEM enrichments for singular pressure and velocity in Darcy flow model. If possible, emphasize a good approximation of the velocity field.
- Suggest new data structures and algorithms for the realization phase in the software Flow123d.

The accuracy of the velocity field, is in the main focus in most applications, e.g. when the flow model is coupled with a transport equation.

At first, a 1d-2d model with XFEM resolving point singularities in pressure based on [2, 3] is developed. Different XFEMs [4, 5] are investigated. Then a model for the same problem in the mixed-hybrid form is derived based on [6]. A new enrichment for velocity is suggested and implemented in Flow123d. The model is further extended into 1d-3d coupled model.

1.3 Document Structure

The thesis is divided into five major parts. In Chapter 2, the reduced dimension concept is described in details and the meshes of combined dimensions are defined. The models of groundwater flow, coupling non-planar 1d-2d and 1d-3d domains, are formulated and put in the context of the software Flow123d and other works.

The background research on various XFEMs is provided in Chapter 3. It is then followed by Chapter 4 where a well-aquifer pressure model is studied and in which the singular enrichments are applied by the means of the XFEM. Various aspects and properties of the model and the method are studied, different enrichment strategies are compared.

Next, the mixed-hybrid model for pressure and velocity is formulated in Chapter 5. A new enrichment for velocity is proposed in the mixed form. The coupled models both for non-planar 1d-2d and 1d-3d are defined and followed by several numerical tests demonstrating the properties of the new enrichment in XFEM.

Chapter 6 is dedicated to the intersection algorithms. The concept of Plücker coordinates is introduced and algorithms for various intersection cases of simplicial elements is described. Numerical experiments are provided.

The thesis is closed with the conclusions in the last Chapter 7 which is followed by the list of author's publications and the bibliography.

2 Reduced Dimensional Models

In this chapter, the concept of combining models of different spatial dimension is introduced. The thesis is put into the context of the so called *reduced dimensional models* and the long-term research at the Technical University of Liberec concentrated around the software Flow123d. Finally, a well aquifer model which is to be solved in this work is defined, combining 1d-2d and 1d-3d dimensions.

The equivalent continuum concept includes the fractures and wells in the model by changing the global properties of the modeled volume (e.g. increased/decreased hydraulic conductivity). This homogenization approach smears local effects of the disruptions but the model can still provide a valid approximation for an initial global view of the system. Since the underlying computational mesh does not need to represent the small scale objects, the equivalent continuum models can be computationally cheap, but they cannot capture the local effects accurately. The other approach considers the disruptions in a discrete sense, keeping its sizes and properties explicitly in the model. This brings more demanding work at the geometric level, where the disruptions have to be represented so that a suitable computational mesh can be built. A significant simplification in this concept is to reduce the dimension of the local phenomena, if possible, and obtain a reduced dimensional model,

The concept of reduced dimensions is fundamental in the Discrete Fracture Network (DFN) models [7] and in models combining DFN with equivalent continuum. The spacial discretization of such models leads to meshes composed of elements of different dimension, in the fractured porous media context e.g. in [8, 9, 10]. There is a limited number of models for coupling of co-dimension 2: 1d-3d coupling or point intersections in non-planar 1d-2d coupling. Such models solving flow and transport in vascular systems are e.g. in [11] and [12].

In the thesis, a reduced dimensional model for fractured porous media being developed by the means of the software Flow123d is extended by nonplanar 1d-2d and 1d-3d models.

2.1 Mesh of Combined Dimensions

As pointed out before, the reduced dimensional models lead to computations on meshes of combined dimensions. The reduced dimensional concept splits the computational domain into parts of different dimensions Ω_d, $d = 1, 2, 3$. The domains Ω_2 and Ω_1 are polytopic (i.e. polygonal and piecewise linear, respectively). Apart from Chapter 4, the simplicial meshes are considered. The *compatible* (or conforming, matching) meshes satify the compatibility conditions, i.e. the $(d-1)$-dimensional elements are either between d-dimensional elements and match their faces or they extend out of Ω_d.

An incompatible mesh (or non-conforming or non-matching), does not have to satisfy the compatibility conditions and therefore the intersecting domains can be meshed independtly, reducing the requirements on the meshing tools significantly. Then of course the intersections must be computed and the discrete model must deal with the incompatible coupling. Therefore Chapter 6 is dedicated to a development of algorithms for efficient computation of intersections of incompatible meshes.

2.2 Well-Aquifer Model

Wells are considered as straight narrow tubes (cylinders) Ω_C^w of radius ρ_w, indexed by $w \in \mathcal{W} = \{1 \dots W\}$. These are reduced to 1d manifolds Ω_1^w, parameterized using a mapping $\nu_w(t) : [0, 1] \to \Omega_1^w$. A lateral surface of a cylinder Ω_C^w is denoted $\partial\Omega_C^w$.

A steady groundwater flow governed by Darcy's law is considered in all domains. Without any coupling terms, one writes for every dimension

$$\frac{1}{\delta_d} \boldsymbol{K}_d^{-1} \boldsymbol{u}_d + \nabla p_d = 0 \qquad \text{in } \Omega_d \tag{2.1}$$

$$\operatorname{div} \boldsymbol{u}_d = \delta_d f_d \qquad \text{in } \Omega_d \tag{2.2}$$

where $\delta_d \boldsymbol{u}_d$ $[ms^{-1}]$ is the unknown Darcian velocity, p_d $[m]$ is the unknown pressure. Parameter δ_d is the complement measure of the domain: thickness $[m]$ in 2d, cross-section $[m^2]$ in 1d and $\delta_3 = 1$ $[-]$ for consistency. Since the wells are considered as cylinders, the cross-section δ_1 is constant per well: $\delta_1(\boldsymbol{x}) = \delta_1^w = \pi\rho_w^2$ for all $\boldsymbol{x} \in \Omega_1^w$. The quantity $\boldsymbol{u}_d$ $[m^{d-4}s^{-1}]$ itself can be seen as flux density, i.e. flux through Ω_d with complementary dimension $\delta_d = 1$. The conductivity tensor $\boldsymbol{K}_d$ $[ms^{-1}]$ is generally

3×3 matrix, symmetric and positive definite, possibly representing the anisotropy of the media. In the source term, f_d $[s^{-1}]$ denotes the water source density.

2.2.1 1d-2d Model

A system of aquifers separated by aquitards is considered (based on Gracie and Craig [2, 3]). The aquifers, denoted Ω_2^m, $m \in \mathcal{M} = \{1 \dots M\}$, are underground horizontal layers of permeable rock containing water. The aquifers' boundary consists of three parts $\partial\Omega_2^m = \Gamma_{2D}^m \cup \Gamma_{2N}^m \cup \bigcup_{w\in\mathcal{W}} \Gamma_w^m$, where Dirichlet and Neumann boundary conditions are prescribed and cross-sections of the wells and aquifers $\Gamma_w^m = \Omega_2^m \cap \partial\Omega_C^w$.

If possible, and apparent from context, the domain unions are denoted

$$\Omega_1 = \bigcup_{w\in\mathcal{W}} \Omega_1^w, \quad \Omega_2 = \bigcup_{m\in\mathcal{M}} \Omega_2^m, \quad \Gamma_\# = \bigcup_{m\in\mathcal{M}} \Gamma_\#^m \tag{2.3}$$

with $\#$ being w, $2D$ or $2N$.

On Γ_w^m, a decomposition of an arbitrary function $q \in C(\bar{\Omega}_2^m)$ on average and fluctuation parts is defined, in the same manner as it can be found in [13],

$$q = \langle q \rangle_w^m + \{q\}_w^m \quad \text{on } \Gamma_w^m, \qquad \langle q \rangle_w^m = \frac{1}{|\Gamma_w^m|} \int_{\Gamma_w^m} q \,\mathrm{d}s. \tag{2.4}$$

The definition of the 1d-2d well-aquifer problem follows:

Problem 2.2.1. Find $[\boldsymbol{u}_1, \boldsymbol{u}_2]$ and $[p_1, p_2]$ satisfying

$$\delta_d^{-1} \boldsymbol{K}_d^{-1} \boldsymbol{u}_d + \nabla p_d = 0 \qquad \text{in } \Omega_d,\ d = 1, 2, \tag{2.5a}$$

$$\operatorname{div} \boldsymbol{u}_2 = \delta_2 f_2 \qquad \text{in } \Omega_2, \tag{2.5b}$$

$$\operatorname{div} \boldsymbol{u}_1 = \delta_1 f_1 + f_w \qquad \text{in } \Omega_1^w,\ \forall w \in \mathcal{W}, \tag{2.5c}$$

$$\langle -\delta_2 \boldsymbol{K}_2 \nabla p_2 \cdot \boldsymbol{n} \rangle_w^m = \Sigma_w^m \qquad \forall w \in \mathcal{W},\ \forall m \in \mathcal{M}, \tag{2.5d}$$

$$\{p_2\}_w^m = g_w^m \qquad \forall w \in \mathcal{W},\ \forall m \in \mathcal{M}, \tag{2.5e}$$

$$p_d = g_{dD} \qquad \text{on } \Gamma_{dD},\ d = 1, 2, \tag{2.5f}$$

$$\delta_d \boldsymbol{K}_d \nabla p_d \cdot \boldsymbol{n} = g_{dN} \qquad \text{on } \Gamma_{dN},\ d = 1, 2 \tag{2.5g}$$

where

$$\Sigma_w^m = \delta_2(\boldsymbol{x}_w^m)\sigma_w^m \big(\langle p_2 \rangle_w^m - p_1(\boldsymbol{x}_w^m)\big), \quad f_w = \sum_{m\in\mathcal{M}} |\Gamma_w^m| \, \Sigma_w^m \delta_t(t - t^m).$$

Term $\delta_t(t-t^m)$ is a Dirac delta measure. The average outward flux from the aquifer over Γ_w acts as a positive source term in the well (blue colored terms).

2.2.2 1d-3d Model

In the 1d-3d model, the aquifer is not reduced to a plane but it is represented as a 3d domain Ω_3, with a boundary $\partial\Omega_3 = \Gamma_{3D} \cup \Gamma_{3N} \cup \bigcup_{w\in\mathcal{W}} \Gamma_w$, where Dirichlet and Neumann boundary conditions are prescribed and cross-sections of the wells and aquifers $\Gamma_w = \Omega_3 \cap \partial\Omega_C^w$, analogically to the 1d-2d model.

On Γ_w the average decomposition $w = \langle g\rangle_w + \{g\}_w$ is defined in a similar manner as in the 1d-2d case. However, the average is computed over a circle edge, perpendicular to Ω_1^w, with its center at a point $\nu_w(t) \in \Omega_1^w$

$$\langle g\rangle_w(t) = \frac{1}{2\pi\rho_w}\int_0^{2\pi} g(t+\rho_w \boldsymbol{n}_{\Omega_1^w}(t,\theta))\rho_w \,\mathrm{d}\theta. \tag{2.6}$$

with $\boldsymbol{n}_{\Omega_1^w}(t,\theta)$ being the unit normal vector of Ω_1^w at point $\nu_w(t)$ in the direction determined by the angle θ.

The definition of the 1d-3d problem follows:

Problem 2.2.2. Find $[\boldsymbol{u}_1, \boldsymbol{u}_3]$ and $[p_1, p_3]$ satisfying

$$\begin{aligned}
\delta_d^{-1}\boldsymbol{K}_d^{-1}\boldsymbol{u}_d + \nabla p_d &= 0 && \text{in } \Omega_d,\ d=1,3, && (2.7a)\\
\operatorname{div}\boldsymbol{u}_3 &= \delta_3 f_3 && \text{in } \Omega_3, && (2.7b)\\
\operatorname{div}\boldsymbol{u}_1 &= \delta_1 f_1 + \Sigma_w && \text{in } \Omega_1^w,\ \forall w\in\mathcal{W}, && (2.7c)\\
\langle -\delta_3\boldsymbol{K}_3\nabla p_3\cdot\boldsymbol{n}\rangle_w &= \Sigma_w && \text{in } \Omega_1^w,\ \forall w\in\mathcal{W}, && (2.7d)\\
\{p_3\}_w &= g_w && \forall w\in\mathcal{W}, && (2.7e)\\
p_d &= g_{dD} && \text{on } \Gamma_{dD},\ d=1,3, && (2.7f)\\
\delta_d\boldsymbol{K}_d\nabla p_d\cdot\boldsymbol{n} &= g_{dN} && \text{on } \Gamma_{dN},\ d=1,3 && (2.7g)
\end{aligned}$$

where

$$\Sigma_w(\boldsymbol{x}) = \delta_3\sigma_w(\boldsymbol{x})\big(\langle p_3\rangle_w(\boldsymbol{x}) - p_1(\boldsymbol{x})\big) \quad \boldsymbol{x}\in\Omega_1^w.$$

One can see the dimensional coupling terms highlighted in the blue color. In contrast to the 1d-2d case, $\Sigma_w(\boldsymbol{x})$, $\boldsymbol{x}\in\Omega_1^w$, varies through the well domain.

3 Extended Finite Element Method

A background research on the XFEM is provided in this chapter, describing the fundamentals and giving an overview on the evolution of the XFEM. Different enrichment methods and various types of enrichments are discussed.

3.1 Basic Concept

The history and the early development of the XFEM is well written in an overview article by Fries and Belytschko [14]. The main feature of this method is the extension of a space of polynomial shape functions of the finite element method with a special function, that enables to better approximate some local effects. This is called *enrichment*. The special function (enrichment function) is often non-polynomial and describes discontinuity or singularity, where polynomials leak accuracy.

The XFEM is mainly perceived as a method for local enrichment, which means that the enrichment is applied only in a small subdomain – several elements of the computational mesh close to the local phenomenon. The XFEM solution with a single enrichment is sought in the form

$$u(\boldsymbol{x}) = \sum_{\alpha \in \mathcal{I}} a_\alpha v_\alpha(\boldsymbol{x}) + \sum_{\alpha \in \mathcal{J}} b_\alpha N_\alpha(\boldsymbol{x}) L(\boldsymbol{x}) \tag{3.1}$$

where a_α are the standard FE degrees of freedom and b_α are the degrees of freedom coming from the enrichment, v_α are the standard FE basis shape functions. We denote the index sets $\mathcal{I}$ and $\mathcal{J}$ that contain all indices of the standard and enriched degrees of freedom, respectively. L is the actual enrichment function and N_α is a linear FE basis functions used as the partition of unity $\sum_\alpha N_\alpha(\boldsymbol{x}) = 1$.

3.1.1 Global Enrichment Functions

Two different types of types of enrichments are discussed in this section – discontinuity and singularity. A discontinuity of the quantity of interest can be strong or weak, depending on whether its value or its derivative

is discontinuous. The location of the discontinuity is often described by a level set function, which itself can be a part of searched solution.

A singularity, which is of the main interest in the thesis, is described by a function with singularity concentrated in a single point in 2d or along a line in 3d. It has symmetric radial character and thus it is often defined in polar (2d) or cylindrical (3d) coordinate system. Typical global enrichment function are summarized e.g. in the Natarajan's thesis [15].

3.1.2 Enrichment Zone

The choice of the enrichment zone, i.e. elements that are enriched, depends on the enrichment type. In case of discontinuities, only the nodes of cut elements are enriched.

In case of singularity, the enrichment must well approximate the adjacent high gradients. To this end, the enrichment zone is typically chosen as a radial area in the vicinity of the singularity of fixed (enrichment) radius, which is necessary to obtain optimal convergence rate, discussed e.g. in [4]. The optimal size of the enrichment zone is however not addressed, apart from [16], where an a priori estimate for the enrichment radius dependent on h is provided, although containing an unknown constant. This matter is investigated in detail later in the thesis.

3.2 Enrichment Methods

In this section, different types of available enrichment methods are discussed. In [4, 14] the Corrected XFEM is introduced and the so called *blending* elements (not all element nodes are enriched) and *reproducing* elements (all element nodes enriched) are differentiated. The problem with lack of the partition of unity on the blending elements is addressed and a solution is suggested by means of the *ramp function* $G(\boldsymbol{x})$ in (3.2). $G(\boldsymbol{x})$ is equal 1 on reproducing elements, is a ramp in blending elements and diminishes elsewhere.

$$L(\boldsymbol{x}) = G(\boldsymbol{x}) s_(\boldsymbol{x}), \tag{3.2}$$

$$L_\alpha(\boldsymbol{x}) = G(\boldsymbol{x}) \left[s(\boldsymbol{x}) - s(\boldsymbol{x}_\alpha) \right]. \tag{3.3}$$

Further the *shifted* enrichment is suggested leading to local enrichment function in (3.3), $\boldsymbol{x}_\alpha$ being element nodes.

Next, the Stable Generalized FEM was developed in [5, 17] and applied in an elastic fracture model. This method is supposed to solve the problem with ill-conditioning, which is often met when using enrichments. The local enrichment function on an element T is defined

$$L_\alpha|_T(\boldsymbol{x}) = s(\boldsymbol{x}) - \pi_T(s)(\boldsymbol{x}), \quad \pi_T(s)(\boldsymbol{x}) = \sum_{\beta \in \mathcal{I}_N(T)} N_\beta(\boldsymbol{x}) s(\boldsymbol{x}_\beta). \quad (3.4)$$

where the interpolation π_T is built using the linear shape functions associated with element nodes. It was later shown in [18] that further care must be taken for different enrichment types for this method to yield optimal convergence and not to suffer with ill-conditioning independent of mesh – discontinuity (or singularity) alignment.

3.3 XFEM in Flow Problems on Meshes of Combined Dimensions

There is much less to be found on the usage of the XFEM in the field of flow modeling, especially regarding the dimensions coupling, than in mechanics. Apart from the references on various types of the XFEM in previous sections, several references dealing with fractured porous media are provided, e.g. [19, 20]. However, no model suitable for a singularity approximation using XFEM in groundwater flow i available.

4 Pressure Model with Singularities

In this chapter, the XFEM with different enrichment techniques is applied on a pressure well-aquifer model in 1d-2d case. The problem for the primary unknown is defined, its weak form is derived and the existence of a unique discrete solution is proved. Several important numerical aspects are inspected, mainly an adaptive quadrature and a choice of an enrichment radius with respect to the convergence of the methods.

4.1 Coupled 1d-2d Model (Primary Weak Form)

Problem 2.2.1 is rearranged, velocity $\boldsymbol{u}_d$ is substituted from the Darcy's law and the problem is solved with pressure p_d as the primary unknown quantity.

Considering standard Sobolev space $H^1_0(\Omega_d) = \left\{q_d \in H^1(\Omega_d); q_d|_{\Gamma_{dD}} = 0\right\}$, and taking the Dirichlet boundary condition into account, the trial space V and the test space V_0 are defined

$$V = H^1(\Omega_1) \times H^1(\Omega_2), \tag{4.1}$$

$$V_0 = H^1_0(\Omega_1) \times V_0^1(\Omega_2^1) \times \cdots \times V_0^M(\Omega_2^M), \tag{4.2}$$

with

$$V_0^m(\Omega_2^m) = \left\{q_2 \in H^1_0(\Omega_2^m) : \{q_2\}_w^m = 0, \forall w \in \mathcal{W}\right\} \quad \forall m \in \mathcal{M}. \tag{4.3}$$

The weak solution $p = [p_1, p_2] \in V$ and the test functions $q = [q_1, q_2] \in V_0$ are denoted and the weak problem is defined

Problem 4.1.1. Find $p = p_0 + p_w + p_D \in V$ such that

$$a(p_0, q) = l(q) - a(p_w, q) - a(p_D, q) \qquad \forall q \in V_0 \tag{4.4}$$

where

$$a(p,q) = \int_{\Omega_2} \delta_2 \boldsymbol{K}_2 \nabla p_2 \cdot \nabla q_2 \,\mathrm{d}\boldsymbol{x} + \int_{\Omega_1} \delta_1 \boldsymbol{K}_1 \nabla p_1 \cdot \nabla q_1 \,\mathrm{d}\boldsymbol{x} + \sum_{\substack{w \in \mathcal{W} \\ m \in \mathcal{M}}} |\Gamma_w^m| \, \delta_2 \sigma_w^m (\langle p_2 \rangle_w^m - p_1(\boldsymbol{x}_w^m))(\langle q_2 \rangle_w^m - q_1(\boldsymbol{x}_w^m)) \tag{4.5}$$

$$l(q) = \int_{\Omega_2} \delta_2 f_2 q_2 \,\mathrm{d}\boldsymbol{x} + \int_{\Omega_1} \delta_1 f_1 q_1 \,\mathrm{d}\boldsymbol{x} + \int_{\Gamma_{2N}} g_{2N} q_2 \,\mathrm{d}s + \int_{\Gamma_{1N}} g_{1N} q_1 \,\mathrm{d}s \tag{4.6}$$

for $p_0 \in V_0$ and given $f_d \in L_2(\Omega_d)$ and $g_{dN} \in L_2(\Gamma_{dN})$, $d = 1, 2$, while $p_w, p_D \in V$ are functions chosen such that they satisfy Dirichlet boundary conditions.

For the solution p of Problem 4.1.1 to be unique it is shown, that it is enough to fix the pressure at the top of a single well (e.g. a pumping well where the pressure can be measured), possibly with Neumann boundary condition at the rest of the boundary.

4.2 Discretization

Problem 4.1.1 is discretized using the linear FE and the XFEM enrichment in the aquifers domains in the vicinity of the singularities. The 2d part of the discrete solution is searched in the form

$$p_{2h}(\boldsymbol{x}) = \sum_{\alpha \in \mathcal{I}_{2N}} a_\alpha N_{2\alpha}(\boldsymbol{x}) + \sum_{w \in \mathcal{W}} \sum_{\alpha \in \mathcal{J}_{2N}^w} b_{\alpha w} N_{2\alpha}(\boldsymbol{x}) L_{\alpha w}(\boldsymbol{x}) \tag{4.7}$$

where $\mathcal{J}_{2N}^w \subset \mathcal{I}_{2N}$ denotes the indices of enriched nodes in $\mathcal{T}_2$ by the well w, and the functions $N_{2\alpha} L_{\alpha w}$ are the local enrichment functions, while $N_{2\alpha}$, the linear FE shape functions, are playing the role of PU.

The local enrichment is chosen according to the particular choice of the enrichment type in Section 3.2. The singular global enrichment function is defined below.

The global enrichment function can be obtained from the solution of a local problem on the neighborhood of the well. In this case, it is a logarithmic function radially symmetric around the well cross-section $\boldsymbol{x}_w = [x_w, y_w]$:

$$s_w(\boldsymbol{x}) = \begin{cases} \log(r_w(\boldsymbol{x})) & r_w > \rho_w, \\ \log(\rho_w) & r_w \leq \rho_w, \end{cases} \tag{4.8}$$

where $r_w(\boldsymbol{x}) = \|\boldsymbol{x} - \boldsymbol{x}_w\| = \sqrt{(x - x_w)^2 + (y - y_w)^2}$ is the distance function.

The XFEM and the SGFEM apply the enrichment functions only locally. Due to the radial character, it is natural to consider a circular

enriched domain $Z_w = B_{R_w}(\boldsymbol{x}_w)$ of the well w given by the enrichment radius R_w. Four different enrichments are defined according to Section Section 3.2: *standard XFEM*, *ramp function XFEM*, *shifted XFEM* and *SGFEM*; which are later compared.

In order to compute the entries of the system matrix, the expressions containing the enrichment functions have to be integrated accurately. There are two aspects which the integration must handle properly:

- the steep gradient of enrichment shape functions in the vicinity of the singularity,
- the singularity cut-off edge geometry.

The instability in the integration in [2] is investigated. An asymptotic analysis of the integration error is presented and new adaptive quadrature rules are defined. Additionally, an adaptive quadrature in polar coordinates is suggested.

4.3 Single Aquifer Analytic Solution

A pseudo-analytic solution is defined in this section. Considering multiple singularities in the domain, the solution can be obtained using the superposition principle. The solution is split into singular and regular part and searched in the form

$$p_2 = p_{sin} + p_{reg} = \sum_{j \in \mathcal{W}} a_j \log r_j + p_{reg}. \tag{4.9}$$

The averages $\langle \cdot \rangle_w$ are evaluated numerically.

4.4 Numerical Tests

The model as described in this chapter was implemented in C++ language using the Deal II library [21], , version 8.0. The model implementation and all the XFEM extensions to the standard FE code were suggested by the author. The source is available on GitHub: `https://github.com/Paulie14/xfem_project`.

Two selected results are displayed in Graphs 4.1-4.2 and Figure 4.1. In Graph 4.1, different enrichment methods defined in 4.2 are compared on

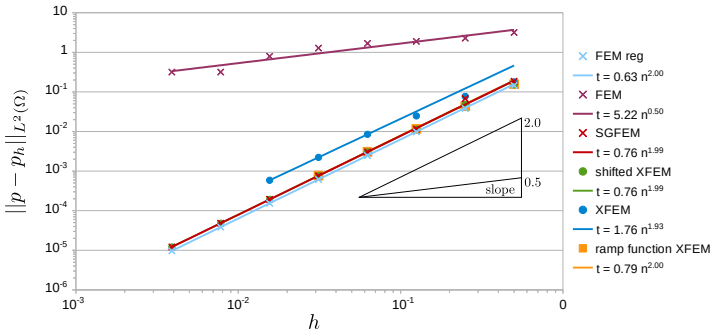

Graph 4.1: Convergence of the L_2 norm of the approximation error.

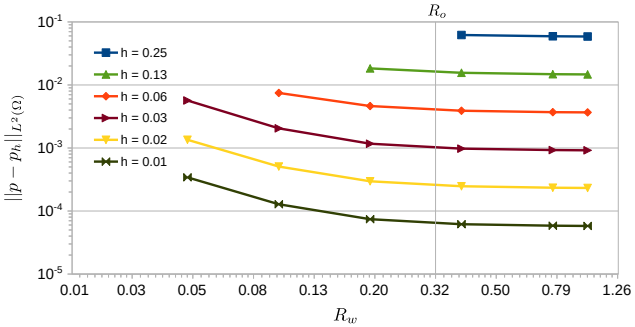

Graph 4.2: Dependence of the error on the enrichment radius for different element sizes h.

a model including a single well and nonzero source term. Optimal convergence order is reached in all XFEMs. The "FEM reg" data comes from the problem without the singularity solved by standard FEM and with optimal convergence order 2.0 for a reference. The standard XFEM displays larger error on blending elements as expected. However, it together with the ramp function XFEM suffers ill-conditioning. The standard FEM converge slowly with order 0.5.

The second Graph 4.2 displays solution error depending on the enrich-

ment radius for different mesh refinements. It shows that the enrichment radius is worth expanding as long as the error of the singular part of the solution is significant in comparison to the error if the regular part. Further increasing of R_w then does not bring increased accuracy. R_o is the optimal enrichment radius where these two error parts are well balanced – theoretical estimate agrees with the numerical result.

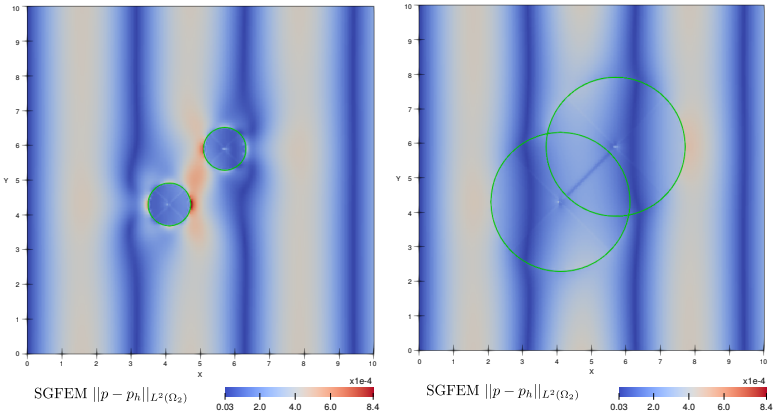

(a) enrichment radius $R_w = 0.6$ (b) enrichment radius $R_w = 2.0$

Figure 4.1: L_2 error distribution in Test case 5 for two different R_w, represented by green circles.

In Figure 4.1 the approximation error is displayed in case of 2 wells and sinusoidal source term along x axis considered. The error of the regular part of the solution is apparent, the error of the singular part is inferior in case of larger enrichment radius. In this problem, the ill-conditioning for shifted XFEM is reported, due to multiple enrichment in the enrichment zone overlap.

5 Mixed Model with Singularities

In this chapter, a mixed hybrid model for Problems 2.2.1 and 2.2.2 is derived, an enrichment for velocity is suggested and numerical experiments in Flow123d are presented, demonstrating the advantages of the approach. The strategic literature, which this chapter is build upon, is listed in the beginning. Foremost the article [6] is mentioned, where the current model of fractured porous media solved in mixed-hybrid form and implemented in Flow123d is described.

5.1 Mixed Dirichlet Problem

At first, a model considering only a 2d aquifer and wells reduced to their cross-sections Γ_w with fixed pressure prescribed as a Dirichlet boundary condition is solved. Its weak form is derived and the existence of a unique continuous solution of the resulting saddle-point problem is shown by the theory in [22].

The derived saddle-point problem is discretized using the hybridization and the lowest Raviart-Thomas FE. The existence and uniqueness of the solution is provided for the unenriched discrete solution.

Then the enrichment of velocity is suggested. The global enrichment function for velocity is the derivative of logarithmic enrichment function introduced in Section 4.2

$$\boldsymbol{s}_w(\boldsymbol{x}) = -\frac{1}{S_e}\frac{\boldsymbol{r}_w}{r_w^2}, \qquad S_e = 2\pi\rho_w. \tag{5.1}$$

where S_e is called an effective (lateral) surface. The properties of $\boldsymbol{s}_w$ are discussed.

An enrichment, where only a single enrichment function is considered per singularity, is suggested. On each enriched element T^i, $i \in \mathcal{J}_E^w$, an SGFEM like interpolation of the global enrichment function, see (3.4), is defined

$$\boldsymbol{L}_w(\boldsymbol{x})|_{T^i} = \boldsymbol{s}_w(\boldsymbol{x}) - \pi_{T^i}^{RT}(\boldsymbol{s}_w)(\boldsymbol{x}). \tag{5.2}$$

where $\pi_{T^i}^{RT}$ is the interpolation operator to standard Raviart-Thomas FE

space. The enriched discrete velocity then takes the form

$$\boldsymbol{u}_h = \sum_{i=1}^{n_F \cdot N_E} a_i \boldsymbol{\psi}_i + \sum_{w \in \mathcal{W}} b_w \boldsymbol{L}_w \tag{5.3}$$

where the first part is the standard approximation (n_F is number of faces per element) and the second part is the enrichment.

A numerical test for inf-sup stability validation is suggested there, to check the LBB condition experimentally, since a theoretical proof is unavailable. A corresponding generalized eigenvalue problem is formulated. However, unclear relation between the mixed and mixed-hybrid form regarding their generalized eigenvalue problems is reported.

Finally, the first numerical results of the 2d Dirichlet problem are presented. Optimal convergence is demonstrated on a series of simple structured simplicial meshes which motivates for further development of the model.

5.2 Coupled 1d-2d Model

The fully coupled mixed-hybrid 1d-2d model is defined. To this end, the following discretization spaces are considered

$$V_h = V_h^{reg}(\Omega_1) \times V_h(\Omega_2), \tag{5.4}$$
$$Q_h = Q_h(\Omega_1) \times Q_h(\Omega_2), \tag{5.5}$$
$$\Lambda_h = \Lambda_h(\mathcal{F}_1) \times \Lambda_h(\mathcal{F}_2) \times \Lambda_h^{enr} \tag{5.6}$$

The velocity space is composed of $V_h^{reg}(\Omega_d)$, $d = 1, 2$, the standard Raviart-Thomas zero order FE space, and $V_h(\Omega_2) = V_h^{reg}(\Omega_2) \oplus V_h^{enr}$, where V_h^{enr} is the enriched space. $Q_h(\Omega_d)$, $d = 1, 2$, is the L_2 space for pressure on elements. $\Lambda_h(\mathcal{F}_d)$, $d = 1, 2$, is the space of Lagrange multipliers in the hybridization (pressure on element faces $\mathcal{F}_d$) and Λ_h^{enr} is the space of average traces of fluxes normal components on the well cross-sections. The saddle point problem then reads:

Problem 5.2.1. Find $\boldsymbol{u}_h = [\boldsymbol{u}_d] \in V_h$ and $p_h = [p_d, \lambda_d, \lambda_w^m] \in Q_h \times \Lambda_h$, $d = 1, 2$, $m \in \mathcal{M}$, $w \in \mathcal{W}$ which satisfy

$$a_h(\boldsymbol{u}_h, \boldsymbol{v}_h) + b_h(\boldsymbol{v}_h, p_h) = \langle G, \boldsymbol{v}_h \rangle_{V_h' \times V_h} \qquad \forall \boldsymbol{v}_h \in V_h, \tag{5.7a}$$
$$b_h(\boldsymbol{u}_h, q_h) - c_w(p_h, q_h) = \langle F, q_h \rangle_{Q_h' \times Q_h} \qquad \forall q_h \in Q_h \times \Lambda_h \tag{5.7b}$$

where the forms are

$$
\begin{aligned}
a_h(\boldsymbol{u}_h, \boldsymbol{v}_h) &= \sum_{\substack{d=1,2 \\ i \in \mathcal{I}_{dE}}} \int_{T_d^i} \delta_d^{-1} \boldsymbol{u}_d \boldsymbol{K}_d^{-1} \boldsymbol{v}_d \,\mathrm{d}\boldsymbol{x}, \\
b_h(\boldsymbol{v}_h, p_h) &= \sum_{\substack{d=1,2 \\ i \in \mathcal{I}_{dE}}} \left[\int_{T_d^i} -p_d \operatorname{div} \boldsymbol{v}_d \,\mathrm{d}\boldsymbol{x}, + \int_{\partial T_d^i \setminus \partial\Omega} \lambda_d (\boldsymbol{v}_d \cdot \boldsymbol{n}) \,\mathrm{d}s \right] \\
&\quad + \sum_{\substack{w \in \mathcal{W} \\ m \in \mathcal{M}}} \int_{\Gamma_w^m} \lambda_w^m \langle \boldsymbol{v}_2 \cdot \boldsymbol{n} \rangle_w^m \,\mathrm{d}s, \\
c_w(p_h, q_h) &= \sum_{\substack{w \in \mathcal{W} \\ m \in \mathcal{M}}} \int_{\Gamma_w^m} \delta_2(\boldsymbol{x}_w^m) \sigma_w^m \left(p_1(\boldsymbol{x}_w^m) - \lambda_w\right) \left(q_1(\boldsymbol{x}_w^m) - \mu_w\right) \mathrm{d}s, \\
\langle G, \boldsymbol{v}_h \rangle_{V_h' \times V_h} &= \sum_{d=1,2} \sum_{i \in \mathcal{T}_d} \int_{\partial T_d^i \cap \Gamma_{dD}} -g_{dD} (\boldsymbol{v}_d \cdot \boldsymbol{n}) \,\mathrm{d}s, \\
\langle F, q_h \rangle_{Q_h' \times Q_h} &= \sum_{d=1,2} \sum_{i \in \mathcal{T}_d} \int_{T_d^i} -\delta_d f_d q_d \,\mathrm{d}\boldsymbol{x},
\end{aligned}
$$

The coupling terms are emphasized in blue color.

5.3 Coupled 1d-3d Model

The 1d-3d coupled model is built in the same manner as the 1d-2d problem.

The well distance function r_w in 3d is defined as a shortest distance between a point and the line representing the well. The enrichment function $\boldsymbol{L}_w$ is suggested in the same form as in 2d and the its properties are demonstrated. The choice of the enrichment zone in 3d is discussed.

Using the same notation as in (5.4)- (5.6) for the discrete space

$$V_h = V_h^{reg}(\Omega_1) \times V_h(\Omega_3), \tag{5.8}$$

$$Q_h = Q_h(\Omega_1) \times Q_h(\Omega_3), \tag{5.9}$$

$$\Lambda_h = \Lambda_h(\mathcal{F}_1) \times \Lambda_h(\mathcal{F}_3) \times \Lambda_h^{enr}, \tag{5.10}$$

the saddle point problem for 1d-3d model is formulated

Problem 5.3.1. Find $\boldsymbol{u}_h = [\boldsymbol{u}_d] \in V_h$ and $p_h = [p_d, \lambda_d, \lambda_w] \in Q_h \times \Lambda_h$, $d = 1, 3$, $w \in \mathcal{W}$ which satisfy

$$a_h(\boldsymbol{u}_h, \boldsymbol{v}_h) + b_h(\boldsymbol{v}_h, p_h) = \langle G, \boldsymbol{v}_h \rangle_{V_h' \times V_h} \qquad \forall \boldsymbol{v}_h \in V_h, \tag{5.11a}$$

$$b_h(\boldsymbol{u}_h, q_h) - c_w(p_h, q_h) = \langle F, q_h \rangle_{Q_h' \times Q_h} \qquad \forall q_h \in Q_h \times \Lambda_h \tag{5.11b}$$

where the forms are

$$a_h(\boldsymbol{u}_h, \boldsymbol{v}_h) = \sum_{\substack{d=1,3 \\ i \in \mathcal{I}_{dE}}} \int_{T_d^i} \delta_d^{-1} \boldsymbol{u}_d \boldsymbol{K}_d^{-1} \boldsymbol{v}_d \, \mathrm{d}\boldsymbol{x},$$

$$b_h(\boldsymbol{v}_h, p_h) = \sum_{\substack{d=1,3 \\ i \in \mathcal{I}_{dE}}} \left[\int_{T_d^i} -p_d \operatorname{div} \boldsymbol{v}_d \, \mathrm{d}\boldsymbol{x}, + \int_{\partial T_d^i \setminus \partial\Omega} \lambda_d (\boldsymbol{v}_d \cdot \boldsymbol{n}) \, \mathrm{d}s \right]$$

$$+ \sum_{w \in \mathcal{W}} \left[2\pi \rho_w \, |\Omega_1^w| \sum_{\substack{i \in \mathcal{I}_{1E} \\ T_1^i \subset \Omega_1^w}} \int_{T_1^i} \lambda_w(t) \langle \boldsymbol{v}_3 \cdot \boldsymbol{n} \rangle_w(t) \, \mathrm{d}t \right],$$

$$c_w(p_h, q_h) =$$

$$\sum_{w \in \mathcal{W}} \left[2\pi \rho_w \, |\Omega_1^w| \sum_{\substack{i \in \mathcal{I}_{1E} \\ T_1^i \subset \Omega_1^w}} \int_{T_1^i} \sigma_w \big(p_1(t) - \lambda_w(t)\big) \big(q_1(t) - \mu_w(t)\big) \, \mathrm{d}t \right],$$

$$\langle G, \boldsymbol{v}_h \rangle_{V_h' \times V_h} = \sum_{d=1,3} \sum_{i \in \mathcal{T}_d} \int_{\partial T_d^i \cap \Gamma_{dD}} -g_{dD} (\boldsymbol{v}_d \cdot \boldsymbol{n}) \, \mathrm{d}s,$$

$$\langle F, q_h \rangle_{Q_h' \times Q_h} = \sum_{d=1,3} \sum_{i \in \mathcal{T}_d} \int_{T_d^i} -\delta_d f_d q_d \, \mathrm{d}\boldsymbol{x}.$$

The coupling terms are again emphasized in blue color.

5.4 Flow123d implementation

Several aspects of the implementation in the software Flow123d is described in this section. Mainly, the changes in the input file format are addressed, adaptive integration and refined output mesh are described.

The adaptive integration strategy is adopted from the pressure model from Chapter 4. Additionally, the quadrature rules are generalized to

all the dimensions, which enables computations on 2d and 3d elements, including integration over their faces which is necessary in the mixed model.

An approach to the visualization of the results containing enriched non-polynomial approximation in VTK format is described. The construction of an adaptively refined output mesh is suggested, in order to display singular enrichments.

5.5 Numerical Tests in Flow123d

5.5.1 Test Cases in 1d-2d

In this section, a set of numerical tests of the 1d-2d model defined in 5.2 is provided. Some of the properties of the velocity enrichment are demonstrated, optimal convergence rate in velocity L_2 error is shown. Different sizes of the enrichment zone are compared.

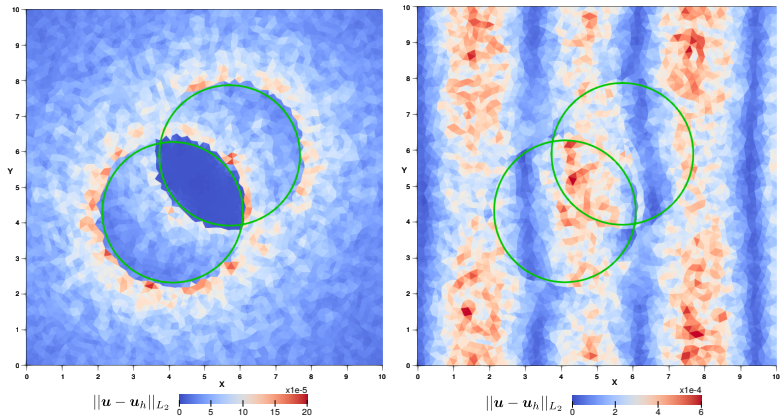

(a) TC2-a (b) TC2-b

Figure 5.1: Test case in 1d-2d. The elementwise L_2 error in velocity is displayed at refinement level 5. The green circle indicates the enrichment radius R_w.

A selected result is displayed in Figure 5.1. It includes 2 wells, perpendicular to the aquifer intersecting it near its center. The enrichment zones overlap each other in the middle, resulting in very small velocity error. The left subfigure corresponds to a problem with zero source term. In the right subfigure, a sinusoidal source term prescribed, the error of the singular part is inferior.

5.5.2 Test Cases in 1d-3d

In this section, a set of numerical tests of the 1d-3d model defined in 5.3 is provided. As in the 1d-2d case, the optimal convergence rate in velocity L_2 error is demonstrated, different sizes of the enrichment zone are compared.

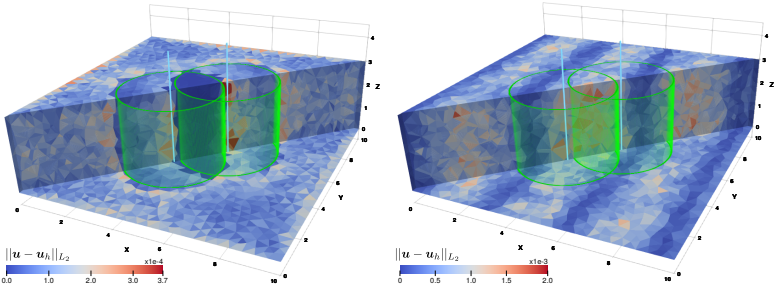

(a) TC5-a (b) TC5-b

Figure 5.2: Test case in 1d-3d. The elementwise L_2 error in velocity is displayed at refinement level 5. The green cylinders indicate the enrichment zone.

A selected result is displayed in Figure 5.2. It has the same setting as the 1d-2d case in 5.5.1, it is however extruded to 3 dimension along the z axis. Lower error can be seen in the enriched zone in the left subfigure, the error of the singular part of the solution is inferior to the error of the regular part in the right subfigure.

Finally, a more complex problem is solved, including 10 wells of different tilt inside of a rock block. A Dirichlet boundary condition is applied on the sides and a zero normal flux boundary condition is set at the bases. An analytical solution is not available in this case, the discrete solution can be inspected qualitatively only, see the solution of velocity Figure 5.3. The block is meshed regularly, the element size can be noticed along the edges of the lower base. The refined solution in the vicinity of the wells is due to the refined output mesh.

The water balance over the domain boundaries can be computed. The relative difference between the flux into and out of the system is below 0.1 %. Thus, we can conclude, that the communication between the wells and the block is well approximated in terms of the water balance.

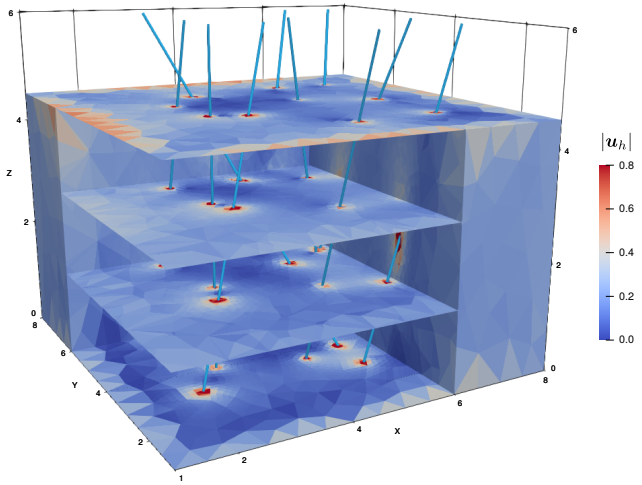

Figure 5.3: Magnitude of velocity in 10 wells problem. Ten wells are represented symbolically by the blue tubes. The block is clipped so that we can see inside.

6 Mesh Intersection Algorithms

In this chapter, the algorithms for intersections of incompatible meshes, which are necessary to our reduced dimensional models, are discussed. Not only the cases 1d-2d, 1d-3d, solved in previous chapters, but a general approach also for cases 2d-3d and 2d-2d is considered. The motivation comes from the future needs for the software Flow123d, to enable computations on incompatible meshes even for fractures. This includes a Mortar like coupling method [23], further development of the XFEM model defined in this thesis, Multilevel Monte Carlo [24] simulations using random fracture generation or time evolving fracture network. The prerequisite for any of these applications is a fast and robust algorithm for calculating intersections of the individual meshes. The content of this chapter includes the results published in the author's article [25].

6.1 Introduction to Mesh Intersection

The research on the currently available algorithms is provided in the introduction. In particular the following are mentioned: the PANG algorithm [26] for 2d-2d and 3d-3d intersections in mesh overlapping problems or 2d-3d intersections algorithm [27] used in the implementation of the Nitche method.

The suggested approach is based on the Plücker coordinates, further developing the algorithm of Platis and Theoharis [28] for ray-tetrahedron intersections. The algorithm is combined with the advancing front method which allows reusing Plücker coordinates and their products among neighboring elements and to reduce the number of arithmetic operations.

6.2 Element Intersections

In this section, the algorithms are presented for computing the intersection of a pair of simplicial elements of a different dimension in a 3d ambient space. The fundamental idea is to compute intersection of 1d-2d simplices using the Plücker coordinates and to reduce all the other cases to this one.

In general, an intersection can be a point, a line segment or a polygon, called *intersection polygon* (IP) in common. IP is represented as a list of points called *intersection corners* (IC). The information about the *topological position* of IC is determined (IC in a vertex, side or face).

Plücker coordinates represent a line in a 3d space. The definition, properties and the more general context from computational geometry can be found e.g. in [29]. It is shown that using Plücker coordinates and their permuted inner product, the relative position of a line and a triangle in ambient 3d space can be determined.

Having computed the Plücker coordinates and all possible permuted inner products in the line-triangle case, this data can be further used to derive the barycentric coordinates of the actual IC. The formula is derived in detail. Then the intersection algorithm for 1d-2d case is suggested, providing also the topological position of the intersection.

Computation of the line-tetrahedron intersection uses the 1d-2d algorithm for each pair line-face. The Plücker coordinates and permuted inner products are computed only once and possibly reused. Each result of 1d-2d algorithm is treated carefully to process the topological positions correctly. Two ICs are returned at most.

In the intersection algorithm in triangle-tetrahedron case, 9 Plücker coordinates (3 sides, 6 edges) and 18 permuted inner products are needed to compute up to 12 side-face intersections and 6 edge-triangle intersections. The result is an n-side intersection polygon (IP), $n \leq 7$. This algorithm is much trickier to obtain correct topological positions of the ICs and to be able to sort them at the end to form a polygon. The algorithm is thoroughly described concerning all possible situations.

The intersection of two triangles uses up to 6 calls of the 1d-2d algorithm for all side-triangle combinations. The algorithm again carefully propagates the topological data from the 1d-2d cases, so that some computations can be skipped. Up to 2 ICs may be found as a result.

6.3 Global Mesh Intersection Algorithm

A composed mesh is considered, containing a 3d mesh, that is called a bulk mesh, and other lower dimensional meshes are called component meshes. At first, all component-bulk mesh intersections are computed, i.e. 1d-3d and 2d-3d. The algorithm includes two steps: finding the first

non-empty element-element intersection (initiation) and prolongation of the intersection using the advancing front tracing.

The search for the initial element-element intersection is accelerated by two techniques. First, the axes align bounding boxes (AABB) are computed for all elements, to provide fast comparison method to detect candidate pairs of elements for the intersection. Second, the bounding interval hierarchy (BIH) [30] can be build upon AABB, to speed up the search.

An advancing front algorithm is suggested to extend the initial intersections, 1d-3d or 2d-3d, looking for candidate pairs among the neighboring component and bulk elements. There it is taken advantage of the topological positions of ICs and the neighboring information on elements. This algorithm runs until the component mesh is covered with all possible bulk elements.

Considering a situation where the component meshes are in the interior of the 3d bulk mesh, the component-bulk results are used for search for candidate pairs in the component-component intersections. The storage of the intersection data, which plays an important part here, is described. On the other hand, component intersections in the exterior of the bulk mesh must be searched via the initiation techniques.

6.4 Benchmarks

In this section, the suggested element-element algorithms are theoretically compared with other available algorithms in terms of floating point operations (FLOPs) count and two numerical benchmarks by the software Flow123d are presented.

6.4.1 Theoretical Comparison

Three algorithms for the line-triangle intersections are compared: Plücker algorithm described in Section 6.2, the algorithm based on the plane clipping due to Haines [31], and the minimum storage algorithm due to Möller and Trumbore (MT) [32]. For the later two algorithms straightforward modifications are considered to make them return a qualitatively same output as our algorithms do.

The estimated numbers of FLOPs for all cases are summarized in Table 6.1. Algorithms based on the Plücker coordinates should be competitive

algorithm	1d-2d	1d-3d	2d-3d
Plücker	92	198	426
Plücker (edge reuse)	45	138	264
Haines	51	177	469
Möller and Trumbore	42	168	756

Table 6.1: Raw number of FLOPs used by different intersection algorithms. Second row contains the estimated effective number of FLOPs per intersection, accounting for reusing the computed Plücker data over neighboring elements, while assuming data on edges of 2d and 3d elements are used twice (conservative).

with the state of the art algorithms in case of 1d-3d and 2d-3d intersections. The expected performance for the 1d-2d case seems to be poor, however these intersections are computed after 1d-3d and 2d-3d, so the Plücker coordinates may be reused. Similarly, better results are expected in the remaining two intersection cases when the Plücker coordinates and their products are reused by neighboring elements.

6.4.2 Global Mesh Intersections

Three variants of the suggested algorithms are compared on 2d-3d benchmarks in this section. The first variant FS+AF uses a full search (FS) over the bulk mesh, i.e. it uses only the unordered array of AABB of elements, to get the initial pair for the advancing front algorithm (AF). The second variant BIH+AF uses the BIH on top of AABB to accelerate the initiation of the AF algorithm. The third variant BIH does not use AF at all and relies on the search through BIH only.

The artificial case considers a composed mesh consisting of a cube and two diagonal rectangular 2d meshes. A sequence of meshes is prepared with an increasing number of elements. All three variants exhibit almost linear time complexity in both the initiation and the intersection phase, relatively to the number of bulk and component elements, respectively. The FS+AF variant is the fastest one, in particular in its initiation phase. the BIH variant is about two times slower than the BIH+AF variant

during the intersection phase.

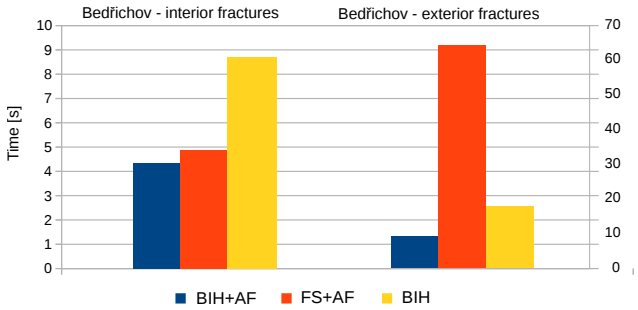

Graph 6.1: Comparison of the algorithms on meshes of Bedřichov locality – interior fractures on the left, extending fractures on the right.

Next, the performance of the intersection algorithms on a mesh of a real locality in Bedřichov in the Jizera mountains is analyzed. Two meshes are considered, one with 28 fractures in the interior of the bulk mesh, the other with artificially extended fractures outside the bulk mesh. The results for both meshes can be seen in Graph 6.1. In the first case, FS+AF and BIH+AF algorithms are nearly twice as fast as BIH. Creating the BIH in the BIH+AF variant pays off and the algorithm performs better than the FS+AF variant. In the second case, a large blow up of the FS+AF variant is caused by the exterior component elements The better performance of both BIH and BIH+AF variants is evident in this case.

Based on the benchmark results, the variant BIH+AF is recommended for general usage, while the FS+AF might be more efficient when there are few component meshes inside a bulk mesh. The algorithms are implemented as a part of the software Flow123d and the results were published in the article [25]. It is currently used in the experimental Mortar model for flow and in the XFEM models presented in Chapter 5.

7 Conclusion

Based on the research of the related works and experience gained at the conferences (in particular MAMERN VI '15, X-DMS '15-17 and CMWR '18), we are convinced that we dedicated our efforts to a very interesting and hot topic with wide range of applications. We are also not aware of any closely connected work to this topic in the Czech Republic which puts us in a pioneer position, in the Czech scientific environment at least.

In the first part of this work, a reduced dimension concept is described and a model for coupling groundwater flow in non-planar 1d-2d and 1d-3d domains intersecting each other is suggested. The drawbacks of several approaches in FE approximation in such models are discussed leading to the suggested solution: incompatible meshing of the domains and using the XFEM to couple them back together and to improve FE approximation of arisen singularities by proper discrete space enrichments.

An extensive study of the currently available XFEM [14, 5] is provided in Chapter 3 and singular enrichments are addressed in particular. Then in Chapter 4, a model simulating pressure in a well-aquifer 1d-2d system, inspired by [2, 3], is created. Different types of enrichments are studied and compared in terms of convergence rate, linear system conditioning and sensitivity to mesh – singularity alignment. In the view of the numerical results, the SGFEM is found to be the most promising method for singularity approximation in the model. Apart from that, several implementation aspects of the XFEM are addressed: improved adaptive quadrature rules for an accurate integration on enriched elements is suggested, optimal enrichment zone for singular enrichments is investigated. The model and methods is verified on a set of numerical test cases. The content of these two chapters is partially summarized in the article [33].

Chapter 5 is dedicated to the XFEM application in a mixed problem in order to extend the possibilities of the groundwater model in [6, 1]. The mixed-hybrid form is carefully derived for both non-planar 1d-2d and 1d-3d case. A new singular SGFEM like enrichment of the standard Raviart-Thomas finite elements is suggested and applied to the velocity discrete space. The model is implemented as an experimental part of the software Flow123d and a set of numerical tests is provided. Since velocity

is important in the attached processes (e.g. transport), a stress is put on the velocity precision and the velocity convergence rate is traced. The optimal order of convergence is observed in both 1d-2d and 1d-3d tests, which included single and multiple wells, overlapping enrichment zones and non-zero source prescribed.

The difficulty of the suggested vector enrichment is that it shares a single degree of freedom per singularity over its whole enrichment zone. This is a source of two problems. First, the system matrix has some non-sparse rows, which can then lead to loosing the sparsity when applying a preconditioner based on elimination. Second, any heterogeneity, e.g. in conductivity, inside the enrichment zone cannot be captured by a single singular enrichment function. We tried to find proper elementwise enrichment functions, similarly to the ones used in the pressure model, however we struggled with the hybridized form, where such enrichment functions must be accompanied by some corresponding Lagrange multipliers. So far we were unsuccessful in performing a numerical test of the inf-sup stability of the mixed-hybrid form, this problem had to be left open. We intend to further study the suggested elementwise enrichment functions and the inf-sup test in the mixed problem without hybridization, however such model is not available in Flow123d yet.

A necessary prerequisite for computations on incompatible meshes is the ability to determine the intersections of the different meshed domains. In Chapter 6 a fast and robust algorithm for computing such intersections on simplicial meshes is developed. Although only the non-planar 1d-2d and 1d-3d cases are necessary in the singular models, the algorithms are extended also to higher dimensions, namely 2d-2d, 2d-3d. New models in these cases are in focus of our future work and further development of the software Flow123d. The properties of the Plücker coordinates [28, 29] are exploited in the element-element intersection algorithms which provide not only the coordinates but also additional topological information. This is then used in the global mesh intersection algorithms together with other modern techniques such as BIH of axes aligned bounding boxes and advancing front tracing. The suggested algorithms are shown to be competitive to other works [32, 31]. The global mesh intersection algorithms are tested in Flow123d on an artificial and a real case benchmarks and they exhibit linear time complexity. The results are summarized in [25]. Possible further improvements include a deeper study on the precision of the used geometric predicates, e.g. regarding the adaptivity in [34], and

thorough code optimization in Flow123d.

The work was also consulted during the author's traineeship at Technical University in Munich at the Department of Numerical Mathematics lead by Prof. Barbara Wohlmuth. Mainly the theoretical aspects of the work and new ideas were discussed. We got also familiarized with a different approach for problems with Dirac delta sources [12, 13] as a coupling method for inclusions.

The goals of this thesis as set in the introduction were fulfilled to a great extent. We studied the XFEM intensively and researched its usage in singular problems. Apart from the created pressure model, we managed to suggest a new velocity enrichment in the mixed-hybrid form and implement a working model in Flow123d. The model was derived and formulated in detail. A lot of technical work was done while preparing all the building blocks for the XFEM in the software. Eventually, we left several open issues which were addressed above.

As we already pointed out, the future work may concern a study of the vector enrichments in the mixed form. Extensions of the discretization for 1d objects that are not straight might be of interest. A specialized iterative method can be suggested in order to solve the linear algebraic system efficiently, including a proper preconditioner. Finally, some processes attached to the groundwater model may be considered using the velocity solution. These processes, namely transport of substances, poroelasticity or heat transfer, then may require similar kind of enrichment for scalar/vector quantities of interest.

8 Author's Publications

Publications

M. Hokr, J. Březina, J. Královcová, J. Říha, P. Exner, I. Hančilová, A. Balvín, Multidimensional Model of Flow and Transport in Fractured Rock for Support of Czech Deep Geological Repository Program, *Proceedings of 2nd International Discrete Fracture Network Engineering Conference, Seattle* (2018), ARMA-DFNE-18-1386,
American Rock Mechanics Association.
`https://www.onepetro.org/conference-paper/ARMA-DFNE-18-1386`.

J. Březina, P. Exner, Fast algorithms for intersection of non-matching grids using Plücker coordinates, *Computers and Mathematics with Applications* 74 (2017) pp. 174-187. ISSN 0898-1221.
`doi.org/10.1016/j.camwa.2017.01.028`.

P. Exner, J. Březina, Partition of unity methods for approximation of point water sources in porous media, *Applied Mathematics and Computation* 273 (2016) pp. 21-32. ISSN 0096-3003.
`doi:10.1016/j.amc.2015.09.048`.

O. Severýn, J. Stebel, P. Exner, Applied mathematics – methodical handbook for AP course, project Education For Effective Transfer Of Technology And Knowledge In Science And Engineering (EE2.3.45.0011), Technical University of Liberec, 2015.

P. Exner, J. Březina, Adaptive integration of singularity in partition of unity methods, in proceedings of *Seminar on Numerical Analysis 2015*, Institute of Geonics AS CR, Ostrava, (2015) pp. 29-32. ISBN 978-80-86407-55-5.
`http://www.ugn.cas.cz/actually/event/2015/sna/sna-sbornik.pdf`.

P. Exner, Partition of unity methods for approximation of point water sources in porous media, in proceedings of *Seminar on Numerical Analysis 2014*, Institute of Computer Science AS CR, Prague, (2014) pp. 29-32. ISBN 978-80-87136-16-4.
`http://www.cs.cas.cz/sna2014/sbornik.pdf`.

Software

J. Březina, J. Stebel, D. Flanderka, P. Exner, J. Hybš, Flow123d, Technical University of Liberec, 2011–2019,
http://flow123d.github.com.

Conferences

DFNE '18, Seattle (US), [presentation]
Multidimensional model of flow and transport in fractured rock for support of Czech DGR program

CMWR '18, Saint Malo (FR), [presentation]
Darcy Flow on Incompatible Meshes of Combined Dimensions

X-DMS '17, Umeå(SE), [presentation]
Singular Enrichment of XFEM on Meshes of Combined Dimensions

HPCSE '17, Soláň (CZ), [poster]
Singular Enrichment in XFEM

FEM Symposium '16, Chemnitz (DE), [presentation]
Extended Finite Element Methods Dealing with Singularities on Meshes of Combined Dimensions

X-DMS '15, Ferrara (IT), [presentation, short course on XFEM attendance]
eXtended Discretization Methods

MAMERN VI '15, Pau (FR), [presentation]
The International Conference on Approximation Methods and Numerical Modeling in Environment and Natural Resources

SNA '15, Ostrava (CZ), [presentation]
Seminar on Numerical Analysis

ESCO '14, Plzeň (CZ), [presentation]
European Seminar on Computing

Stanford, 2014 (US) [attendance only]
40th Stanford Geothermal Workshop

SNA '14, Nymburk (CZ), [presentation]
Seminar on Numerical Analysis

Student conference '13, Liberec (CZ), [poster]
Student conference at the Faculty of Mechatronics, Informatics and Interdisciplinary Studies, Technical University of Liberec

Bibliography

[1] J. Březina, J. Stebel, D. Flanderka, P. Exner, J. Hybš, Flow123d (2011–2019).
URL: http://flow123d.github.com

[2] R. Gracie, J. R. Craig, Modelling well leakage in multilayer aquifer systems using the extended finite element method, *Finite Elements in Analysis and Design* 46 (6) (2010) pp. 504–513. ISSN 0168-874X. doi:10.1016/j.finel.2010.01.006.

[3] J. R. Craig, R. Gracie, Using the extended finite element method for simulation of transient well leakage in multilayer aquifers, *Advances in Water Resources* 34 (9) (2011) pp. 1207–1214. ISSN 0309-1708. doi:10.1016/j.advwatres.2011.04.004.

[4] T.-P. Fries, A corrected XFEM approximation without problems in blending elements, *International Journal for Numerical Methods in Engineering* 75 (5) (2008) pp. 503–532. ISSN 1097-0207. doi:10.1002/nme.2259.

[5] I. Babuška, U. Banerjee, Stable generalized finite element method (SGFEM), *Computer Methods in Applied Mechanics and Engineering* 201–204 (2012) pp. 91–111. ISSN 0045-7825. doi:10.1016/j.cma.2011.09.012.

[6] J. Šístek, J. Březina, B. Sousedík, BDDC for mixed-hybrid formulation of flow in porous media with combined mesh dimensions, *Numerical Linear Algebra with Applications* 22 (6) (2015) pp. 903–929. ISSN 10705325. doi:10.1002/nla.1991.

[7] L. Jing, O. Stephansson, 10 - discrete fracture network (dfn) method, in: L. Jing, O. Stephansson (Eds.), Fundamentals of Discrete Element Methods for Rock Engineering, Vol. 85 of *Developments in Geotechnical Engineering*, Elsevier, 2007, pp. 365 – 398. doi:https://doi.org/10.1016/S0165-1250(07)85010-3.

[8] V. Martin, J. Jaffré, J. E. Roberts, Modeling fractures and barriers as interfaces for flow in porous media, *SIAM Journal on Scientific Computing* 26 (5) (2005) pp. 1667–1691. ISSN 1095-7197. doi:10.1137/S1064827503429363.

[9] A. Fumagalli, A. Scotti, Numerical modelling of multiphase subsurface flow in the presence of fractures, *Communications in Applied and Industrial Mathematics* 3 (1). ISSN 2038-0909. doi:10.1685/journal.caim.380.

[10] J. Březina, J. Stebel, Analysis of model error for a continuum-fracture model of porous media flow, in: High Performance Computing in Science and Engineering. HPCSE 2015, Vol. 9611 of *Lecture Notes in Computer Science*, Springer International Publishing, Cham, 2016, pp. 152–160. ISBN 978-3-319-40361-8. doi:10.1007/978-3-319-40361-8_11.

[11] C. D'Angelo, A. Quarteroni, On the Coupling of 1d and 3d Diffusion-reaction equations: Application to Tissue Perfusion Problems, *Mathematical Models and Methods in Applied Sciences* 18 (08) (2008) pp. 1481–1504. ISSN 0218-2025, 1793-6314. doi:10.1142/S0218202508003108.

[12] T. T. Köppl, Multi-scale modeling of flow and transport processes in arterial networks and tissue, Ph.D. thesis, Technical University of Munich, Germany (2015).

[13] T. Köppl, E. Vidotto, B. Wohlmuth, P. Zunino, Mathematical modeling, analysis and numerical approximation of second-order elliptic problems with inclusions, *Mathematical Models and Methods in Applied Sciences* 28 (05) (2018) pp. 953–978. doi:10.1142/S0218202518500252.

[14] T.-P. Fries, T. Belytschko, The extended/generalized finite element method: An overview of the method and its applications, *International Journal for Numerical Methods in Engineering* 84 (3) (2010) pp. 253–304. ISSN 1097-0207. doi:10.1002/nme.2914.

[15] S. Natarajan, Enriched finite element methods: Advances and applications, Ph.D. thesis, Cardiff University, United Kingdom (Jun. 2011).

[16] V. Gupta, C. A. Duarte, On the enrichment zone size for optimal convergence rate of the generalized/extended finite element method, *Computers and Mathematics with Applications* 72 (3) (2016) pp. 481 – 493. ISSN 0898-1221. doi:https://doi.org/10.1016/j.camwa.2016.04.043.

[17] V. Gupta, C. A. Duarte, I. Babuška, U. Banerjee, A stable and optimally convergent generalized FEM (SGFEM) for linear elastic fracture mechanics, *Computer Methods in Applied Mechanics and Engineering* 266 (2013) pp. 23–39. ISSN 0045-7825. doi:10.1016/j.cma.2013.07.010.

[18] Q. Zhang, I. Babuška, U. Banerjee, Robustness in stable generalized finite element methods (sgfem) applied to poisson problems with crack singularities, *Computer Methods in Applied Mechanics and Engineering* 311 (2016) pp. 476 – 502. ISSN 0045-7825. doi:https://doi.org/10.1016/j.cma.2016.08.019.

[19] A. Fumagalli, Numerical modelling of flows in fractured porous media by the XFEM method, Ph.D. thesis, Polytechnic University of Milan, Italy (2012).

[20] N. Schwenck, B. Flemisch, R. Helmig, B. I. Wohlmuth, Dimensionally reduced flow models in fractured porous media: crossings and boundaries, *Computational Geosciences* 19 (6) (2015) pp. 1219–1230. ISSN 1573-1499. doi:10.1007/s10596-015-9536-1.

[21] W. Bangerth, R. Hartmann, G. Kanschat, Deal.II—a general-purpose object-oriented finite element library, *ACM Trans. Math. Softw.* 33 (4). ISSN 0098-3500. doi:10.1145/1268776.1268779.

[22] F. Brezzi, M. Fortin (Eds.), Mixed and Hybrid Finite Element Methods, Vol. 15 of *Springer Series in Computational Mathematics*, Springer, New York, 1991. ISBN 978-1-4612-7824-5 978-1-4612-3172-1.

[23] J. Březina, Mortar-like mixed-hybrid methods for elliptic problems on complex geometries, in: Conference proceedings of Algoritmy 2012, Slovak University of Technology in Bratislava, 2012, pp. 200–208. ISBN 978-80-227-3742-5.

[24] M. B. Giles, Multilevel Monte Carlo methods, *Acta Numerica* 24 (2015) pp. 259–328. ISSN 0962-4929, 1474-0508. doi:10.1017/S096249291500001X.

[25] J. Březina, P. Exner, Fast algorithms for intersection of non-matching grids using plücker coordinates, *Computers & Mathematics with Applications* 74 (2017) pp. 174 – 187. ISSN 0898-1221. doi:10.1016/j.camwa.2017.01.028.

[26] M. J. Gander, C. Japhet, Algorithm 932: PANG: Software for nonmatching grid projections in 2d and 3d with linear complexity, *ACM Transactions on Mathematical Software* 40 (1) (2013) pp. 1–25. ISSN 00983500. doi:10.1145/2513109.2513115.

[27] A. Massing, M. G. Larson, A. Logg, Efficient implementation of finite element methods on nonmatching and overlapping meshes in three dimensions, *SIAM Journal on Scientific Computing* 35 (1) (2013) pp. C23–C47. ISSN 1064-8275, 1095-7197. doi:10.1137/11085949X.

[28] N. Platis, T. Theoharis, Fast ray-tetrahedron intersection using plucker coordinates, *Journal of graphics tools* 8 (4) (2003) pp. 37–48. doi:10.1080/10867651.2003.10487593.

[29] M. Joswig, T. Theobald, Plücker coordinates and lines in space, in: Polyhedral and Algebraic Methods in Computational Geometry, Springer London, London, 2013, pp. 193–207. ISBN 978-1-4471-4817-3. doi:10.1007/978-1-4471-4817-3_12.

[30] C. Wächter, A. Keller, Instant ray tracing: The bounding interval hierarchy, in: Proceedings of the 17th Eurographics Conference on Rendering Techniques, EGSR '06, Eurographics Association, Aire-la-Ville, Switzerland, Switzerland, 2006, pp. 139–149. ISBN 3-905673-35-5. doi:10.2312/EGWR/EGSR06/139-149.

[31] E. Haines, V.1 - fast ray – convex polyhedron intersection, in: Graphics Gems II, Morgan Kaufmann, San Diego, 1991, pp. 247 – 250. ISBN 978-0-08-050754-5. doi:10.1016/B978-0-08-050754-5.50053-0.

[32] T. Möller, B. Trumbore, Fast, minimum storage ray-triangle intersection, *Journal of Graphics Tools* 2 (1) (1997) pp. 21–28. ISSN 1086-7651. doi:10.1080/10867651.1997.10487468.

[33] P. Exner, J. Březina, Partition of unity methods for approximation of point water sources in porous media, *Applied Mathematics and Computation* 273 (2016) pp. 21–32. ISSN 0096-3003. doi:http://dx.doi.org/10.1016/j.amc.2015.09.048.

[34] J. Richard Shewchuk, Adaptive precision floating-point arithmetic and fast robust geometric predicates, *Discrete & Computational Geometry* 18 (3) (1997) pp. 305–363. ISSN 1432-0444. doi:10.1007/PL00009321.